CHALLENGES IN AMORPHOUS SILICON SOLAR CELL TECHNOLOGY[*]

R. A. C. M. M. van Swaaij, M. Zeman, B. A. Korevaar, C. Smit, J. W. Metselaar
Delft University of Technology, Laboratory of Electronic Components, Technology and Materials - DIMES, P. O. Box 5053, NL-2600 GB Delft, Netherlands

M. C. M. van de Sanden
Eindhoven University of Technology, Department of Applied Physics, P. O. Box 513, NL-5600 MB Eindhoven, Netherlands

Hydrogenated amorphous silicon is nowadays extensively used for a range of devices, amongst others solar cells. Solar cell technology has matured over the last two decades and resulted in conversion efficiencies in excess of 15%. In this paper the operation of amorphous silicon solar cells is briefly described. For tandem solar cell, amorphous silicon germanium is often used as material for the intrinsic layer of the bottom cell. This improves the red response of the cell. In order to optimize the performance of amorphous silicon germanium solar cells, profiling of the germanium concentration near the interfaces is applied. We show in this paper that the performance is strongly dependent on the width of the grading near the interfaces. The best performance is achieved when using a grading width that is as small as possible near the p-i interface and as wide as possible near the i-n interface. High-rate deposition of amorphous silicon is nowadays one of the main issues. Using the Expanding Thermal Plasma deposition method very high deposition rates can be achieved. This method has been applied for the fabrication of an amorphous silicon solar cell with a conversion efficiency of 5.8%.

1 Introduction

Devices based on hydrogenated amorphous silicon (a-Si:H) have matured considerably over the last decade. This material is now for instance used for photo-conductive layers in electrophotography, for thin film transistors (TFTs), and not in the least for solar cells. Since the first a-Si:H solar cell was made by Carlson *et al.* [1] the technology has improved tremendously, leading to reported initial efficiencies exceeding 15% [2].

In this paper we will first outline the basic operation principles of a-Si:H solar cells based on a single p-i-n structure and highlight problems that are specifically related to a-Si:H solar cells, i.e., the light-induced degradation that leads to performance degradation of the solar cell.

[*]Presented at the Workshop on Solid State Surfaces and Interfaces II, Bratislava, Slovakia, June 20 – 22, 2000.

Current high efficient solar cells are based on the so-called multi-junction and multi-band gap approach, i.e., a stack of two or more single p-i-n cells. Advantages of this structure are that each component cell can be tuned to a specific part of the solar spectrum and that each cell is thinner and therefore less sensitive to light-induced defect creation. The tuning of the response to the solar spectrum is usually achieved by alloying the amorphous silicon with Ge, thereby lowering the optical band gap of the material. In this paper we will show how the cell's response can be optimized by profiling the Ge concentration in the intrinsic layer of the device. The dependencies of the external parameters on the Ge profile will be examined and these give some clues of the physics underlying a layer with a band-gap profile.

To date *a*-Si:H solar cells are mainly produced by employing the so-called Plasma Enhanced Chemical Vapour Deposition (PECVD) process. This process has been successfully applied for the production of large areas. However, for high volume production a typical deposition rate of 2 Å/s is somewhat low and therefore considerable research effort is devoted to high-rate deposition of *a*-Si:H layers and devices. We will show results of material and solar cell devices deposited with an Expanding Thermal Plasma. With this technique deposition rates of up to 10 nm/s can be achieved. We will address problems that are related to the device optimization of solar cells made with this deposition method.

2   Amorphous silicon solar cell

The operation of an *a*-Si:H solar cell is somewhat different to that of a crystalline silicon cell due to the different material properties. Therefore we will first summarize some material characteristics of *a*-Si:H, as this is important for the understanding of the design and operation of the solar cell. For a more thorough description we refer to Ref. 3 and references therein.

A-Si:H is mainly characterized by the lack of long-range order. There is, however, still short-range order, i.e., most silicon atoms have four neighbours in a (nearly) diamond like structure. As a result of the short-range order *a*-Si:H has a band structure and the common semiconductor concept of conduction and valence bands can be used. The absence of long-range order, however, means that these bands are not sharp and have tails that extent into the band gap. Physically these band tails represent energy levels of strained silicon-silicon bonds, resulting from bond-angle and/or bond-length distributions. The width of these band tails is more or less a measure for the amount of disorder in the material. In addition to the band tails there is a quasi-continuum of states throughout the band tails related to broken bonds, usually referred to as dangling bonds. These dangling bonds can capture charge carriers and can seriously limit the conductivity of the material. Fortunately most of these dangling bonds are passivated by hydrogen that is incorporated during the deposition process and the dangling bond density is reduced from about 10^{21} cm^{-3} in pure *a*-Si (amorphous silicon that contains no hydrogen) to 10^{15} cm^{-3}, i.e., less than 1 dangling bond per million atoms. Although hydrogenated amorphous silicon contains more hydrogen than defects, still not all the defects are passivated. Currently, the general consensus is that there is an equilibrium between the width of the tail states (i.e. the density of weak or strained Si-Si bonds) and the defect density [4]. The tail states and the dangling bonds have a large effect on the electronic properties of *a*-Si:H, in particular the diffusion length. An important property of *a*-Si:H is its direct band gap. As a result the absorption of this material in the visible wavelength region is about 100 times higher than that of crystalline silicon, which has an indirect

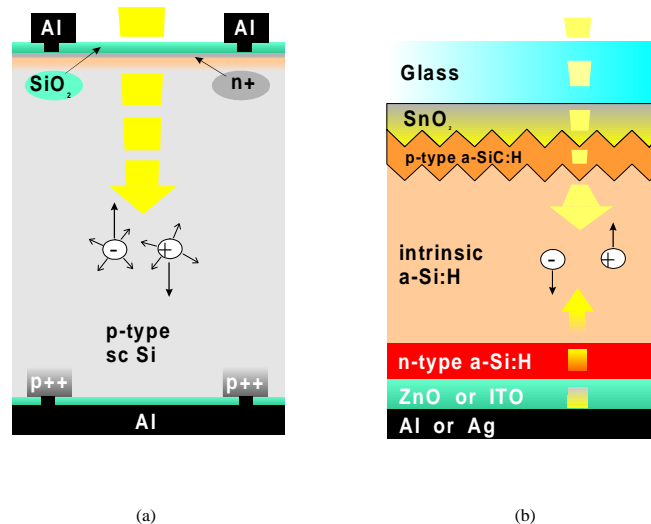<div align="center">(a)</div> <div align="center">(b)</div>

Fig. 1. Schematic representation of (a) a crystalline silicon solar cell and (b) an amorphous silicon solar cell.

band gap. As will be explained below, this is one of the major advantages of this material for solar cells.

Solar cell operation is based on the photo-voltaic effect, i.e. the absorption of photons that generate electron-hole pairs in the semiconductor material. A crystalline silicon solar cell, shown in Fig. 1a, consists of a p- and an n-type layer that form a p-n junction. In this case electron-hole pairs are generated in the 100 to 300 μm thick and electrically neutral p-layer. The electrons, the minority carriers in the p-type layer, diffuse towards the junction and in the depletion region near the junction the electrons drift to the n-layer under the influence of an internal electric field. This device is called a diffusion device as the carriers reach the junction between the p- and the n-type layer by diffusion. The diffusion length of minority carriers (i.e. electrons in p-type material) in *a*-Si:H is too low for practical operation and therefore a solar cell based on *a*-Si:H is designed differently. A schematic lay-out of an *a*-Si:H solar cell is shown in Fig. 1b. In this case the active device consists of three layers: a p-type *a*-SiC:H layer, an intrinsic (i.e. undoped) *a*-Si:H layer, and an n-type *a*-Si:H layer. Because the intrinsic layer is sandwiched in between the doped layers, an internal electric field is present across the intrinsic layer and this layer is therefore depleted of charge carriers. The electron-hole pairs are in this case generated in the intrinsic *a*-Si:H layer and are immediately separated by the internal electric field. The carriers then drift under the influence of the internal electric field to the electrodes and therefore an *a*-Si:H solar cell is called a drift device.

Some other key features of *a*-Si:H solar cells also become apparent in Fig. 1b: (i) As substrate, glass covered with transparent conductive oxide (TCO) is used, e.g. SnO$_2$:F or ZnO. In order to obtain high efficiency solar cells, this TCO is generally textured as a result of which the incoming light is scattered and the absorption in the solar cell is enhanced. (ii) The carri-

ers generated in the p-type layer that is deposited on top of the TCO do not contribute to the photocurrent and it is thus desirable that the light absorption in that layer is small. A smaller absorption (i.e. a higher optical band gap) is achieved by alloying the *a*-Si:H with carbon. The p-type layer is therefore sometimes referred to as a window layer [5]. (iii) The thickness of the amorphous silicon solar cell is comparable to the thickness of the depletion region in the crystalline silicon solar cell, i.e., about 0.5 μm. As mentioned above, this small thickness can be allowed because *a*-Si:H has a direct band gap as a result of which the absorption of this material is higher. The small thickness implies an enormous reduction in material and energy consumption during production, and in weight of solar cell modules (specifically for space applications) when compared to crystalline silicon solar cells. (iv) The cell is completed by the back electrode that often consists of a ZnO layer followed by a back metal, usually Ag, on top of the n-type *a*-Si:H layer. It has been shown that this combination results in a highly reflective back contact leading to an improved red response of the cell.
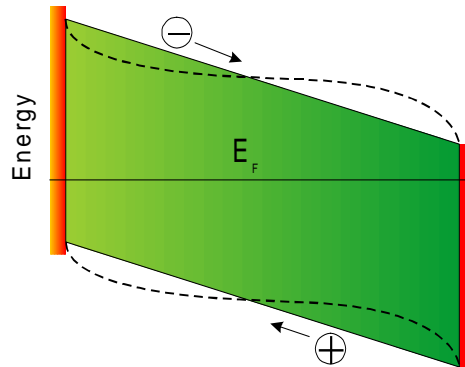

Fig. 2. A simple band diagram of an amorphous silicon solar cell. As a result of defect creation strong band bending occurs near the interfaces and the internal electric field in the intrinsic layer is distorted (dashed line).

Inherent to *a*-Si:H is the creation of defects when the material is illuminated [6]. This so-called Staebler-Wronski effect is undesirable for solar cells, because these additionally created defects will trap photo-generated charge carriers as they drift towards the electrodes. As a result of the trapping a space charge region develops in the intrinsic *a*-Si:H layer and the internal electric field is distorted (see Fig. 2), which in turn leads to lower drift and thus to a lower collection efficiency. The process is reversible by annealing the cell at moderate temperatures and is repeated when the cell is again illuminated. The degradation can be partly compensated by using thinner intrinsic layers in which case the internal electric field is higher and therefore less sensitive to any distortion. However, the total light absorption in the solar cell will then decrease. The solution to obtain cells with a better stability is a tandem or a multi-junction structure. The total thickness of the complete structure is the same as for a single junction solar cell, but each component cell is thinner and therefore less sensitive to light-induced defects. An additional advantage of a tandem structure is that each component cell can be tailored to a specific part of

the solar spectrum, thereby improving the performance even more. The tailoring is realized by implementing amorphous silicon germanium (*a*-SiGe:H) as material for the intrinsic layer of the bottom cell. Recently, an initial conversion efficiency in excess of 15% has been demonstrated on laboratory scale with this approach of multi-junction, multi-band gap structures [2].

Several issues are related to the tandem cell approach. First of all, the tandem cell is in fact a series connection of current sources. The component cell that is generating the smallest current determines the current generated in the complete cell. It is thus required that each component cell generates the same current and therefore the thickness of the intrinsic layer of each component cell needs to be carefully adjusted, thereby taking the generation profile in the cell into account. Secondly, the interface between the component cells is in fact p-n diode, which is connected in reverse direction compared to the component cells. In order for the tandem cell to operate properly an ohmic contact between the component cells is required. The problem can be resolved by implementing a so-called tunnel-recombination junction. This junction ensures that the electron current from the top cell and the hole current from the bottom cell recombine at this junction. A tunnel-recombination junction is realized by using microcrystalline silicon for at least one of the doped layers and/or to increase the defect density at the interface between the two component cells. The lower band gap of the microcrystalline material and a large defect density at this interface results in a high recombination probability.

In the following section we will pay attention to the *a*-SiGe:H solar cell. This material has a lower optical band gap and a solar cell employing this material for the intrinsic layer shows a better red response. Therefore this solar cell is used as the bottom cell in a tandem cell structure. In Section 4 we will discuss the deposition of amorphous silicon. Especially, we will focus our attention to a new deposition method and with which very high deposition rates can be achieved. This method has been developed at Eindhoven University of Technology and is currently being investigated at Delft University of Technology for the potential of solar cell fabrication.

3   Profiled a-SiGe:H solar cells

As explained above, the use of *a*-SiGe:H for the intrinsic layer of the bottom cell in a tandem structure enhances the red response of the cell because of the lower optical band gap of this material. However, when Ge is incorporated in the material this is accompanied by an increase in the defect density and if used for the intrinsic layer of a solar cell this leads to a performance reduction [7, 8]. An additional problem of using *a*-SiGe:H are the large band offsets near the p-i and i-n interfaces. These band offsets are believed to obstruct an effective collection of photo-generated carriers. In order to overcome this, profiling of the Ge concentration in a region near the interfaces has been demonstrated to be very successful [9, 10]. Here we will give a brief overview of the dependencies of the external parameters (i.e. the conversion efficiency, η, the short- circuit current, J_{sc}, the open-circuit voltage, V_{oc}, and the fill factor, *FF*) on the width of the profiling.

The solar cells were deposited in a three-chamber plasma enhanced chemical vapor deposition (PECVD) set-up. Samples enter the system via a load lock, thereby achieving that the reaction chambers can maintain a high vacuum. The intrinsic layers are grown in a separate chamber in order to avoid cross contamination with the doping gases used for the deposition of the p- and n-type layers. High-quality material can be made in this system, which is supported by

the fact that single junction *a*-Si:H test solar cells have an initial energy conversion efficiency of more than 10% [11]. The *a*-SiGe:H was deposited using a high hydrogen dilution ($[H_2]/([SiH_4]$ + $[GeH_4]) = 39$) in order to obtain optimal material quality. Other important deposition conditions are listed in Table 1. The band gap in the intrinsic layer was profiled by adjusting the $[GeH_4]/[SiH_4]$ gas flow ratio during the deposition by varying the SiH_4 and GeH_4 gas flow. Throughout the deposition of the profiled *a*-SiGe:H layer the hydrogen dilution was maintained at 39. When varying the p-i (i-n) grading width the i-n (p-i) grading width is kept at 15 (25) nm. The thickness of the intrinsic layer of the device, including the grading, is 150 nm in all cases and the band gap is varied from 1.8 eV to 1.5 eV.

Deposition temperature (°C)	190
Deposition pressure (mbar)	2.0
Power density (mW/cm^2)	13

Table 1. Important deposition parameters.

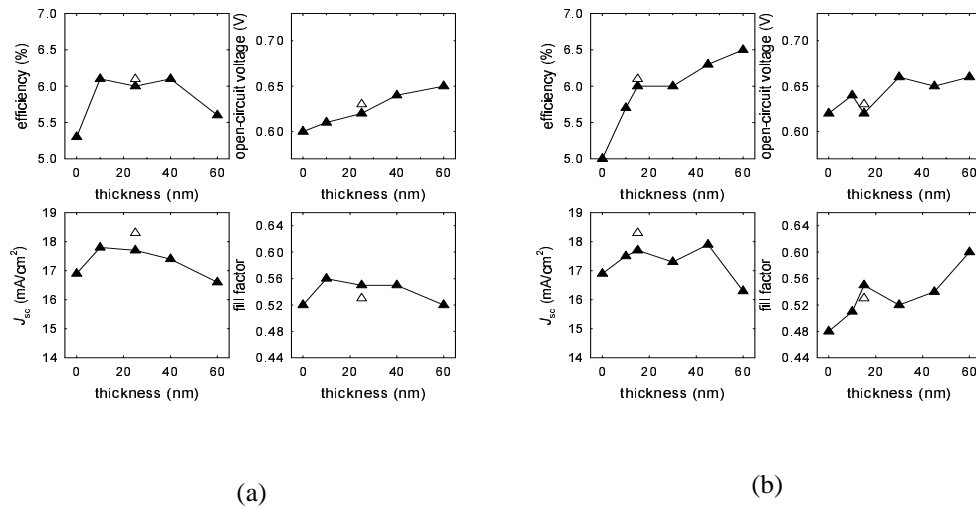(a)   (b)

Fig. 3. The dependence of the external solar cell parameters for AM1.5 illumination as a function of the profiling width near the (a) p-i interface and (b) i-n interface.

The dependence of the external parameters as a function of the grading width near the p-i and i-n interfaces is shown in Fig. 3. As expected, applying a grading is beneficial for the performance of the solar cell. However, the dependence on the grading width near the p-i interface (Fig. 3a) shows a different behaviour to that near the i-n interface (Fig. 3b). Under AM1.5 illumination an increase of the p-i grading width does not improve the efficiency and even decreases this for

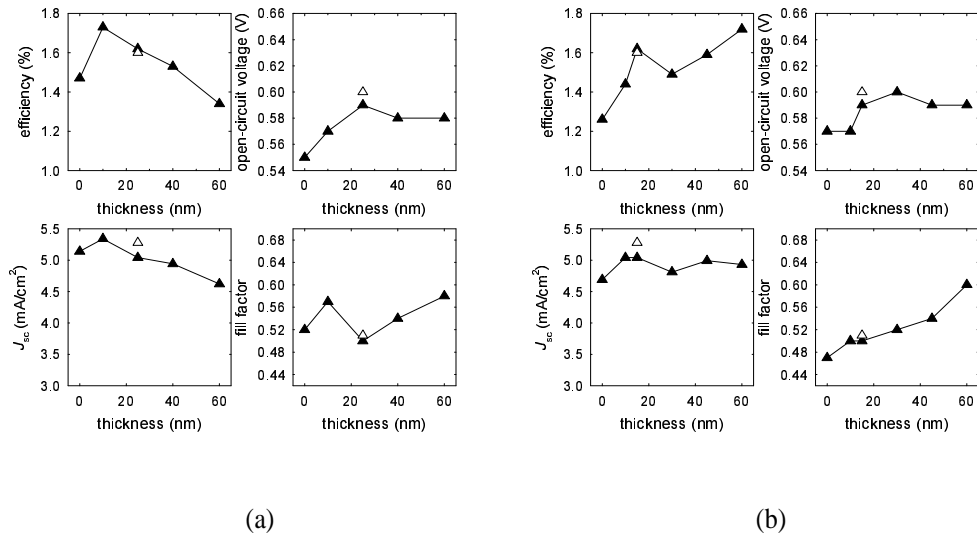(a)   (b)

Fig. 4. The dependence of the external solar cell parameters for filtered AM1.5 illumination ($\lambda > 640$ nm) as a function of the profiling width near the (a) p-i interface and (b) i-n interface.

large widths, mainly due to a drop in the short- circuit current density, J_{sc}, and the fill factor, *FF*. The opposite is observed for the efficiency when the i-n grading width is changed, because the *FF* improves. The J_{sc} is hardly affected and only decreases for a very large grading width. In both cases the open- circuit voltage, V_{oc}, increases. As presented in Fig. 4, these effects become even more pronounced in the red part of the spectrum ($\lambda > 640$ nm), to which the *a*-SiGe:H solar cell response should be tuned. In that case the efficiency decreases drastically upon p-i grading reflecting the reduction of J_{sc}, whereas i-n grading greatly improves the efficiency because the collection of photo-generated carriers is better as concluded from the increasing *FF*. For p-i as well as i-n grading the V_{oc} increases with increasing width of the graded layer for $\lambda > 640$ nm, but saturates above a particular width. In conclusion, the best performance is obtained when making the p-i grading width as small as possible and the i-n grading as large as possible. However, note that the p-i grading cannot be omitted.

Based on the above results, an *a*-SiGe:H solar cell with optimal grading widths of $d_{p-i} = 10$ nm, $d_{i-n} = 45$ nm, and total thickness $d_{tot} = 150$ nm has been made and the J, V curve is shown in Fig. 5. For comparison also a curve is presented in case *no* Ge profiling is applied near the interfaces. This optimized cell showed an $\eta = 7.6\%$, with the other parameters: $J_{sc} = 18.0$ mA/cm^2, $V_{oc} = 0.68$ V, and *FF* = 0.62. It should be mentioned that this performance is achieved *without* using a ZnO back reflector, which is known to enhance particularly the J_{sc} considerably.
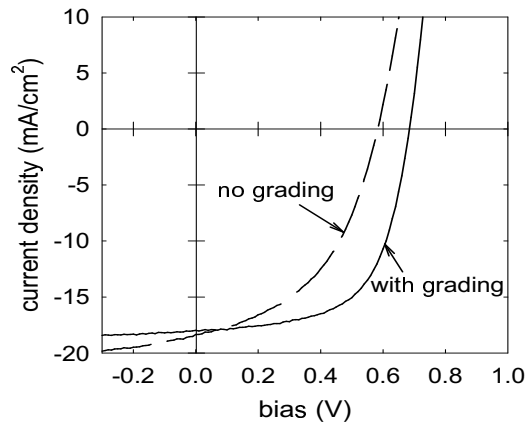
Fig. 5. The J, V curve of an a-SiGe:H solar cell based on an optimal grading profile. Also shown the J, V curve of an a-SiGe:H in which *no* Ge profiling is applied.

4   High-rate deposition of a-Si:H

In general thin layers of a-Si:H are deposited by rf PECVD at 13.56 MHz. The deposition is realized by letting silicon-containing gas, usually silane (SiH_4), into a vacuum chamber. The substrate serves as the grounded electrode and a radio-frequent (13.56 MHz) voltage is fed to the opposite electrode. In between the electrodes a plasma is created and a flux of radicals and ions is directed towards the substrate on which a film is deposited. Due to the nature of this process the SiH_4 gas can easily be mixed with other gases which will result in material with different properties. For instance, in order to make p-type material diborane (B_2H_6) is added to the gas mixture and boron is incorporated in the material. Also other properties can be easily manipulated. Adding germane (GeH_4) or methane (CH_4) to the gas mixture results in material with a lower or higher band gap, respectively. This flexibility is strongly employed for the production of more efficient solar cells. A major drawback of this technique is the relatively low deposition rate. For high-efficiency solar cells good quality material is required and this is obtained at deposition rates of less than 5 Å/s, implying that the time required depositing a solar cell is at least 15 minutes. It is obvious that the low deposition rates limit the high volume production of solar cells. In addition, for a roll-to-roll deposition system employing PECVD large vacuum chambers are needed. Therefore several methods are investigated with which a-Si:H can be deposited at high rates, e.g., Hot-Wire CVD.

At Eindhoven University of Technology a plasma deposition method has been developed and with which deposition rates in excess 100 Å/s have been demonstrated. The deposition set-up for the so-called Expanding Thermal Plasma (ETP) is shown in Fig. 6. The set-up consists of a dc thermal-arc plasma source and a low-pressure chamber. The plasma production and deposition are geometrically separated and this system is therefore regarded as a remote-plasma system [12]. The plasma is generated by a dc discharge (typically 50 A, 100 V) between three cathodes and
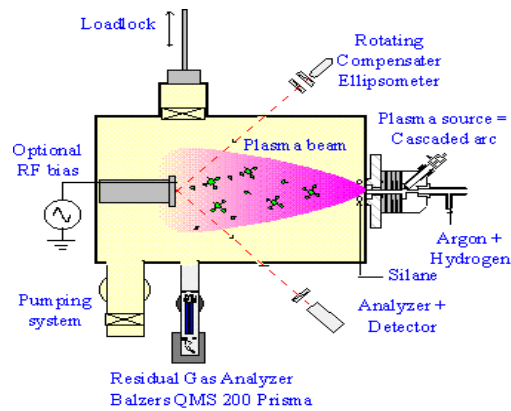
Fig. 6. A schematic representation of the Expanding Thermal Plasma deposition system.

an anode. As the arc is operated at a typical pressure of 0.5 bar, the plasma is close to local thermal equilibrium and characterized by a high electron density and low electron temperature ($n_e \approx 10^{22}$ m^{-3}, $T_e \approx 1$ eV). It can flow into the deposition chamber through a conical shaped nozzle in the anode plate. Usually a gas mixture of argon and hydrogen is used resulting primarily in a flux of atomic hydrogen.

The plasma expands supersonically into the deposition chamber (pressure typically 0.2 mbar), shocks and flows subsonic towards the substrate. Near the substrate the plasma beam has a diameter of about 10 cm, which depends on the deposition pressure. In the Ar-H$_2$ plasma jet typical downstream plasma parameters are an electron density of about 10^{17} m^{-3} and an electron temperature of about 0.2 eV. Pure SiH$_4$ is injected into the plasma jet just behind the expansion nozzle.

Due to the low electron temperature, the substrate self bias is less than 2 V, which means that the ion bombardment is negligible. It also rules out dissociation of SiH$_4$ by electron collisions; the dissociation is mainly attributed to hydrogen abstraction. If no H$_2$ is added to the arc the H abstraction is mainly due to Ar ions emanating from the arc, resulting in relatively large contribution of SiH$_2$ to the film deposition. In the case of cascaded arc deposition this results in porous material with poor conductive properties. By adding H$_2$ to gas mixture in the arc the Ar ions are quenched and atomic H mainly drives the H-abstraction from SiH$_4$ from the arc. This leads in SiH$_3$ being the main depositing species and appears to result in much better material.

The deposition rate is dependent on a number of factors, like the pressure in the deposition chamber. In Fig. 7a the dependence of the deposition rate as a function of the SiH$_4$ flow is shown for two different deposition temperatures. Clearly, the deposition rate increases rapidly when the SiH$_4$ flow is enhanced, but does not depend on the deposition temperature. The quality of the material as a function of deposition rate is another matter and we refer for a more elaborate discussion to Ref. 13. In Fig. 7b we have plotted the refractive index, which we take as a measure for the material quality, as a function of the deposition rate for two different deposition temperatures.
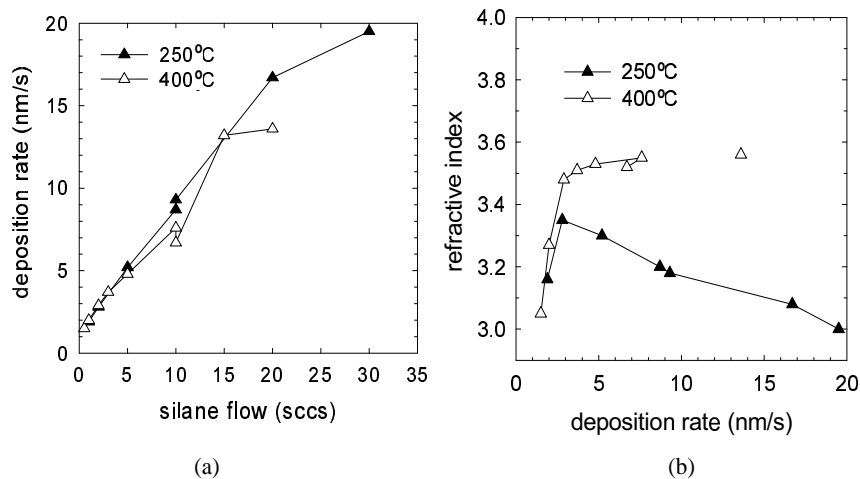
Fig. 7. (a) The deposition rate as a function of the silane flow in the injection ring and (b) the refractive index as a function of the deposition rate.

It now appears that the refractive index as a function of the deposition rate shows a maximum for the lower deposition temperature. For higher rates the refractive index decreases, indicating that the quality of the material deteriorates. However, the refractive index of material deposited at 400 °C above a deposition rate of 3 nm/s is more or less independent of the deposition rate.

In order to employ the ETP deposition method for solar cells, a system has been built at Eindhoven University of Technology and installed at Delft University of Technology, called CASCADE, in which a complete solar cell can be fabricated. The system consists of three chambers: a rf PECVD chamber for the deposition of the doped layers, an ETP chamber for the high-rate deposition of the intrinsic layer, and a load-lock. With this set-up it is ensured that no vacuum breaks are required in between the deposition of the individual layers. The doped layers are produced using PECVD, because an accurate control of the thickness of these layers is essential and thus a fairly low deposition rate is desired. So far optimization runs have been carried out in order to obtain good-quality material. For solar cell applications the photosensitivity, defined as the ratio of the photo-conductivity and the dark conductivity, of the material is an important parameter. The photosensitivity depends strongly on the quality of the material, i.e., the defect density. In Fig. 8 the deposition-rate dependence of the photosensitivity is plotted. This figure shows that a particular photosensitivity at a chosen deposition rate can only be obtained above a certain deposition temperature. This finding implies that for high-rate deposition, high deposition temperatures are required. A high deposition temperature for the intrinsic layer can 'damage' the p-type a-SiC:H, usually leading to a drop in the blue response of the cell. Before deposition of the intrinsic layer, the p-type layer is exposed to the higher deposition temperature and as a result hydrogen leaves the material. The lower hydrogen content in turn leads to material with a lower band gap.

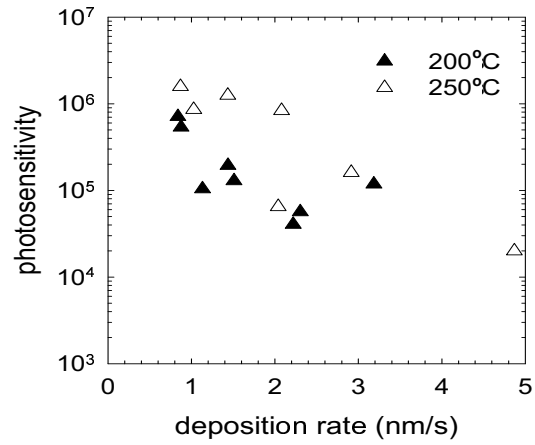The best solar cell that has been made so far in joint CASCADE project is shown in Fig. 9.

Fig. 8. The deposition-rate dependence of the photosensitivity of material deposited in CASCADE at 200 °C and 250 °C.

This cell has a conversion efficiency of 5.8%, J_{sc} = 13.7 mA/cm^2, V_{oc} = 0.74, and FF = 0.57. In this case the p-type layer was deposited at a temperature of 170 °C and the intrinsic layer was deposited at a rate of 0.87 nm/s. Although the ETP material has similar properties to PECVD
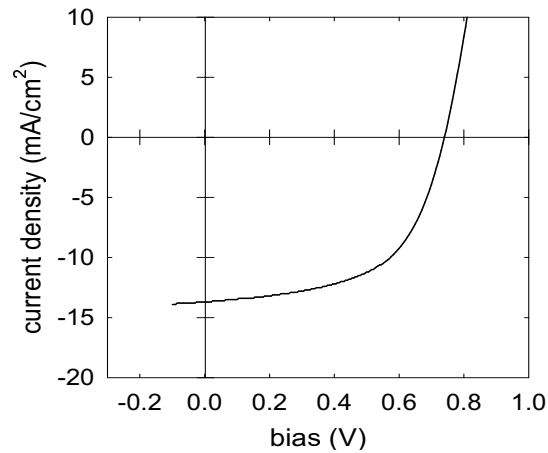

Fig. 9. J, V curve of a solar cell deposited at a rate of 0.87 nm/s. This solar cell has a conversion efficiency of 5.8%, J_{sc} = 13.7 mA/cm^2, V_{oc} = 0.74, and FF = 0.57.

material the solar cell performance is somewhat low. Currently we investigate the underlying cause of this effect.

5   Conclusions

In this paper we have presented the basic operation principles of amorphous silicon solar cells. Inherent to amorphous silicon is the light-induced defect creation, resulting in a performance drop of the device. Making a stack of thinner solar cells (multi-junction) partly overcomes this degradation in performance. Also in this way the complete device can be better tuned to the solar spectrum. Therefore amorphous silicon germanium is used as low band gap material for the bottom cell in a tandem structure.

It is shown that grading of the Ge concentration near the p-i and i-n interfaces improves the performance of amorphous silicon germanium solar cells. For an optimal performance the grading width near the p-i interface needs to be as small as possible and the width near the i-n interface as large as possible.

One of the main challenges at this moment is the fast deposition of amorphous silicon. We are investigating a novel deposition technique for the fast deposition of solar cells: the Expanding Thermal Plasma. With this method deposition rates for amorphous silicon in excess of 10 nm/s have been demonstrated. With this technique we have fabricated a solar cell with an efficiency of 5.8% at a deposition rate of 0.87 nm/s.

References

[1] D.E. Carlson, C.R. Wronski: *Appl. Phys. Lett.* **28** (1976) 671

[2] J. Yang, A. Banerjee, K. Lord, S. Guha: in *Proceedings of the 2nd World Conference and Exhibition on Photovoltaic Solar Energy Conversion*, edited by J. Schmid, H.A. Ossenbrink, P. Helm, H. Ehmann, E.D. Dunlop, Vienna, Austria, 6-10 July, 1998, p. 387

[3] R.A. Street: *Hydrogenated amorphous silicon*, Cambridge University Press, 1991

[4] M.J. Powell, S.C. Deane: *Phys. Rev. B* **53** (1996) 10121

[5] Y. Tawada, H. Okamoto, Y. Hamakawa: *Appl. Phys. Lett.* **39** (1981) 237

[6] D.L. Staebler, C.R. Wronski: *Appl. Phys. Lett.* **31** (1977) 292

[7] M. Stutzmann, R.A. Street, C.C. Tsai, J.B. Boyce, S. E. Ready: *J. Appl. Phys* **66** (1989) 569

[8] G.H. Bauer: *Solid State Phenomena* **44-46** (1995) 365

[9] S. Guha, J. Yang, A. Pawlikiewicz, T. Glatfelter, R. Ross, S.R. Ovshinsky: *Appl. Phys. Lett.* **54** (1989) 2330

[10] J. Fölsch, D. Lundszien, F. Finger, H. Stiebig, J. Zimmer, C. Beneking, S. Wieder, H. Wagner: in *Proceedings of the 14th European Photovoltaic Solar Energy Conference*, edited by H.A. Ossenbrink, P. Helm, H. Ehmann, Barcelona, Spain, 30 June - 4 July, 1997, p. 601

[11] M. Zeman, R.A.C.M.M. van Swaaij, E. Schroten, L.L.A. Vosteen, J.W. Metselaar: *Mater. Res. Soc. Symp. Proc.* **507** (1998) 409

[12] M.C.M. van de Sanden, R.J. Severens, W.M.M. Kessels, F. van de Pas, L. van IJzendoorn, D.C. Schram: *Mater. Res. Soc. Symp. Proc.* **467** (1997) 621

[13] A.J.M. Smets, C. Smit, B.A. Korevaar, W.M.M. Kessels, D.C. Schram, M.C.M. van de Sanden: *Mater. Res. Soc. Symp. Proc.* (2000) to appear